Ceramics International 49 (2023) 1–40

CERAMICS INTERNATIONAL

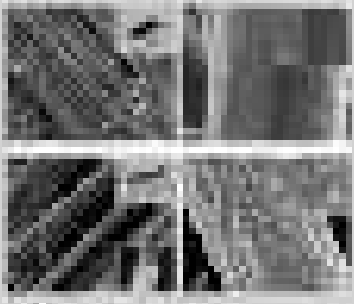

Submit Your Paper (https://www.editorialmanager.com/ceri)

Supports Open Access (https://www.elsevier.com/journals/ceramics-international/0272-8842/open-access-options)

View Articles (https://www.sciencedirect.com/science/journal/02728842)

Guide for Authors

Abstracting/ Indexing (http://www.elsevier.com/journals/ceramics-international/0272-8842/abstracting-indexing)

Track Your Paper

Order Journal (https://www.elsevier.com/journals/institutional/ceramics-international/0272-8842)

Journal Metrics

› CiteScore: **6.1** ⓘ

Impact Factor: **3.830** ⓘ

5-Year Impact Factor: **3.513** ⓘ

Source Normalized Impact per Paper (SNIP): **1.310** ⓘ

SCImago Journal Rank (SJR): **0.891** ⓘ

› View More on Journal Insights

(https://sdgresources.relx.com/)

Help expand a public dataset of research that support the SDGs. (https://www.elsevier.com/connect/help-expand-a-public-dataset-of-research-that-support-the-un-sdgs)

Your Research Data

› Share your research data (https://www.elsevier.com/authors/author-resources/research-data)

Related Links

› Researcher Academy

› Author Resources (https://www.elsevier.com/authors/author-resources)

Ceramics International - Editorial Board

General Editor

P. Vincenzini

World Academy of Ceramics, National Research Council, Faenza, Italy

Editors-in-Chief

R.K. Bordia

Clemson University, Clemson, South Carolina, United States

Z. Fu

Wuhan University of Technology, Wuhan, China

T. Ohji

National Institute of Advanced Industrial Science and Technology Advanced Manufacturing Research Institute, Tsukuba, Japan

V.C. Pandolfelli (https://www.journals.elsevier.com:443/ceramics-international/editorial-board/vc-pandolfelli)

Federal University of Sao Carlos Department of Materials Engineering, SAO CARLOS, Brazil

R. Riedel

Technical University of Darmstadt Department of Materials and Earth Sciences, Darmstadt, Germany

Associate Editors

M. Ferrari, PhD
National Research Council Institute of Photonics and Nanotechnologies Branch of Trento, Trento, Italy

A. Łukowiak
Institute of Low Temperature and Structure Research Polish Academy of Sciences, Wroclaw, Poland

Z.J. Yu
Xiamen University, Xiamen, China

Editorial Board

University of Padova Department Industrial Engineering, Via Marzolo 9, 35131, Padova, Italy

R. Danzer

University of Mining, 8700, Leoben, Austria

B. Derby

The University of Manchester, M13 9PL, Manchester, United Kingdom

D.K. kim

Korea Advanced Institute of Science and Technology, 335 Gwahangno (373-1 Guseong-dong), Yuseong-gu, 305-701, Daejeon, Korea, Republic of

A. Dominguez-Rodriguez

University of Seville Department of Condensed Matter Physics, Apartado 1065, 41080, Sevilla, Spain

M. Dondi

Institute of Science and Technology of Ceramic Materials National Research Council, via Granarolo 64, 48018, Faenza, Italy

J. Dusza

Institute of Materials Research of SAS, 4001, Kosice, Slovakia

M.F. Ferreira

University of Aveiro, Campus Universitário, 3810-193, Aveiro, Portugal

J.R. Frade

University of Aveiro Department of Economics Management Industrial Engineering and Tourism, 3810-191, Aveiro, Portugal

N. Frage

Ben-Gurion University of the Negev, 84105, Be'er Sheva, Israel

W.L. Gladfelter
University of Minnesota Department of Chemistry, 207 Pleasant Street S.E, Minneapolis, Minnesota, 55455-0431, United States

T. Graule
Empa Materials Science and Technology, CH-8600, Dübendorf, Switzerland

H.J. Hannink
CSIRO Australian Manufacturing and Materials Precinct, Normandy Road, Clayton, 3168, Australia

T. Ishikawa
Sanyo-Onoda City University, 756-0884, Sanyoonoda, Japan

S.J.L. Kang
Korea Advanced Institute of Science and Technology, 335 Gwahangno (373-1 Guseong-dong), Yuseong-gu, 305-701, Daejeon, South Korea

M. Kawashita
Tohoku University International Research Institute of Disaster Science, Sendai, Japan

H-D. Kim
Korea Institute of Materials Science Engineering Ceramics Research Department, 531 Changwondaero, 641-831, Changwon, Korea, Republic of

Y.W. Kim
University of Seoul, Dongdaemun-gu, 02504, Seoul, Korea, Republic of

J.C. Knowles
University College London, WC1E 6BT, London, United Kingdom

W. Krenkel
University of Bayreuth Department of Ceramic Materials Engineering, Ludwig-Thoma-Strasse 36b, D-95447, Bayreuth, Germany

J. Lamon, PhD (https://www.journals.elsevier.com:443/ceramics-international/editorial-board/j-lamon-phd)
Laboratory of Mechanics and Technology, 61 avenue du President Wilson, 94235, Cachan, France

Y. Li
Wuhan University of Technology, 430070, Wuhan, China

H. Lin
Oak Ridge National Laboratory, Oak Ridge, Tennessee, 37831-2008, United States

J. Lis
AGH University of Science and Technology Faculty of Materials Science and Ceramics, Al. Mickiewicza Adama 30,

W. Sigmund
University of Florida Department of Materials Science and Engineering, 225 Rhines Hall, P.O. Box 116400, Gainesville, Florida, 32611-6400, United States

M. Singh
NASA John H Glenn Research Center, MS 106-5 Ceramic Branch, Cleveland, Ohio, OH 44135-3191, United States

G. Srinivasan
Oakland University, Rochester, Michigan, 48309-4401, United States

D. Suvorov
Jozef Stefan Institute, 1000, Ljubljana, Slovenia

T. Troczynski
The University of British Columbia, Vancouver, V6T 1Z4, British Columbia, Canada

W.H. Tuan
National Taiwan University Department of Materials and Science Engineering, No. 1, Sec. 4, Roosevelt Road, 10617, Taipei, Taiwan

A. Vinu
The University of Newcastle, University Drive, Callaghan, Newcastle, NSW 2308, New South Wales, Australia

M. Wang
University of Hong Kong Department of Mechanical Engineering, 7/F, Haking Wong Building, Pokfulam Road, Hong Kong, Hong Kong

S. Yin
Tohoku University, 2-1-1 Katahira, Aoba-ku, Miyagi, Japan

N. Zhou
Henan University of Technology, Luoyang, China

Y. Zhou
Chinese Academy of Sciences, 100864, Beijing, China

Y. Zhou
Harbin Institute of Technology Institute of Advanced Ceramics, 92 West Dazhi Street, Nan'gang District, 150001, Harbin, China

All members of the Editorial Board have identified their affiliated institutions or organizations, along with the corresponding country or geographic region. Elsevier remains neutral with regard to any jurisdictional claims.

Ceramics International

Readers
View Articles
Volume/ Issue Alert

Ceramics International

Supports *open access*

Search in this journal

6.1 CiteScore

3. In

Volume 47, Issue 6

Pages 7293-8742 (15 March 2021)

Previous vol/issue

Next vol/issue

Receive an update when the latest issues in this journal are published

Sign in to set up alerts

Reviews

Review article ○ Abstract only

Chromium poisoning for prolonged lifetime of electrodes in solid oxide fuel cells - Review

Teruhisa Horita

Pages 7293-7306

Purchase PDF Article preview

Review article ○ Abstract only

Laser surface texturing of ceramics and ceramic composite materials – A review

Alessandro De Zanet, Valentina Casalegno, Milena Salvo

Pages 7307-7320

Purchase PDF Article preview

Review article ○ Abstract only

Review MXenes as a new type of nanomaterial for environmental applications in the photocatalytic degradation of water pollutants

Xiaofang Feng, Zongxue Yu, Yuxi Sun, Runxuan Long, ... Jianghai Liu

Pages 7321-7343

Purchase PDF Article preview

Ceramics International

Supports *open access*

6.1 CiteScore 3. In

Review article ○ Abstract only

Light-activated room-temperature gas sensors based on metal oxide nanostructures: A review on recent advances

Jing Wang, Huchi Shen, Yi Xia, Sridhar Komarneni

Pages 7353-7368

Purchase PDF Article preview

Review article *Open access*

Incorporation of organic liquids into geopolymer materials - A review of processing, properties and applications

Charles Reeb, Christel Pierlot, Catherine Davy, David Lambertin

Pages 7369-7385

Download PDF Article preview

Original Articles

Research article ○ Abstract only

A comparative study of the structural, optical, magnetic and magnetocaloric properties of $HoCrO_3$ and $HoCr_{0.85}Mn_{0.15}O_3$ orthochromites

Komal Kanwar, Indrani Coondoo, M. Anas, Vivek K. Malik, ... Neeraj Panwar

Pages 7386-7397

Purchase PDF Article preview

Research article ○ Abstract only

The milling effect of a new horizontal attrition milling in the production of $(Ti_{0.7},W_{0.3})C$–Ni cermet

Daegwon Ha, Jae-Hee Kim, Moonsu Seo

Pages 7398-7406

Purchase PDF Article preview

Research article ○ Abstract only

Optical dispersion analysis of template assisted 1D-ZnO nanorods for optoelectronic applications

Kebadiretse Lefatshe, Phindani Dube, Dineo Sebuso, Morgan Madhuku, Cosmas Muiva

Pages 7407-7415

Purchase PDF Article preview

Research article ○ Abstract only

Synthesis of manganese (IV) oxide at activated carbon on reduced graphene oxide sheets via laser irradiation technique for organic binder-free electrodes in flexible supercapacitors

Talal F. Qahtan, Emre Cevik, Mohammed A. Gondal, Ayhan Bozkurt, ... Muhammad Hassan

Pages 7416-7424

Purchase PDF Article preview

Ceramics International

Supports *open access*

6.1 CiteScore 3. In

Research article ○ Abstract only

Revisiting structural evolution, dielectric and ferroelectric properties in $(Pb_xBa_{1-x})ZrO_3$ system ($0.5 \leq x \leq 1.0$)

Feng Li, Mingsheng Long, Chunchang Wang, Jiwei Zhai

Pages 7430-7437

Purchase PDF Article preview

Research article ○ Abstract only

Zn–Mn-ptcda derived two-dimensional leaf-like $Zn_{0.697}Mn_{0.303}Se$/C composites as anode materials for high-capacity Li-ion batteries

Jiaoyu Xiao, Hongdong Liu, Yao Lu, Lei Zhang, Jiamu Huang

Pages 7438-7447

Purchase PDF Article preview

Research article ○ Abstract only

Zirconia-strengthened yttria ceramics for plasma chamber applications

Yicheng Tan, Jingtong Zhang, Peng Chen, Zuoxiang Zhu, ... Zhuo Tian

Pages 7448-7456

Purchase PDF Article preview

Research article ○ Abstract only

Synthesis of hollow maghemite (<gamma>-Fe_2O_3) particles for magnetic field and pH-responsive drug delivery and lung cancer treatment

Sheng Li, Renzi Zhang, Daoxin Wang, Li Feng, Kang Cui

Pages 7457-7464

Purchase PDF Article preview

Research article ○ Abstract only

Densification behaviour and three-dimensional printing of Y_2O_3 ceramic powder by selective laser sintering

A. Ratsimba, A. Zerrouki, N. Tessier-Doyen, B. Nait-Ali, ... G. Delaizir

Pages 7465-7474

Purchase PDF Article preview

Research article ○ Abstract only

Electrochemical performance of quaternary $(1-x)ZnMn_2O_4/(x)MgFe_2O_4$ solid solution as supercapacitor electrode

Zein K. Heiba, M.A. Deyab, A.M. El-naggar, Mohamed Bakr Mohamed

Pages 7475-7486

Purchase PDF Article preview

Research article ○ Abstract only

Friction behavior of PTFE-coated Si_3N_4/TiC ceramics fabricated by spray technique under dry friction

Wenlong Song, Shoujun Wang, Yang Lu, Xuan Zhang, Zixiang Xia

Ceramics International

Supports *open access*

6.1 CiteScore 3.

M. Moreno Amado, J.J. Olaya, J.E. Alfonso

Pages 7497-7503

Purchase PDF Article preview

Research article ○ Abstract only

Performance of Al2O3 particle reinforced glass-based seals in planar solid oxide fuel cells

Ruizhu Li, Jiajun Yang, Dong Yan, Jian Pu, ... Jian Li

Pages 7504-7510

Purchase PDF Article preview

Research article ○ Abstract only

Systematic study on mechanical and electronic properties of ternary VAlN, TiAlN and WAlN systems by first-principles calculations

Lei Chen, Junlian Xu, Meiguang Zhang, Taotao Rong, ... Peifang Li

Pages 7511-7520

Purchase PDF Article preview

Research article ○ Abstract only

Development of multilayer graded cemented carbides with Ti–Zr carbonitride miscibility gaps

Na Li, Qiwei Wang, Weibin Zhang, Yong Du, ... Yajun Li

Pages 7521-7527

Purchase PDF Article preview

Research article ○ Abstract only

Preparation and gas-sensing performance of GO/SnO_2/NiO gas-sensitive composite materials

Lili Jiang, Sihao Tu, Kang Xue, Haitao Yu, Xingang Hou

Pages 7528-7538

Purchase PDF Article preview

Research article ○ Abstract only

Dielectric properties and electromagnetic wave transmission performance of aluminium silicate fibreboard at 915 MHz and 2450 MHz

Xiaobiao Shang, Di Zhai, Meihong Liu, Junruo Chen, ... Guangchao Li

Pages 7539-7557

Purchase PDF Article preview

Research article ○ Abstract only

Stabilizing nanocrystalline Cu_2O with ZnO/rGO: Engineered photoelectrodes enables efficient water splitting

Arunkumar Shanmugasundaram, Muhammad Ali Johar, Ramireddy Boppella, Dong-Su Kim, ... Dong Weon Lee

Pages 7558-7570

Purchase PDF Article preview

Ceramics International

Supports *open access*

6.1 CiteScore 3. Im

Research article ○ Abstract only

Medium-entropy $(Ti, Zr, Hf)_2SC$ MAX phase

Ke Chen, Youhu Chen, Jianning Zhang, Yujie Song, ... Qing Huang

Pages 7582-7587

Purchase PDF Article preview

Research article ○ Abstract only

Re-examination of phase relations between solid solutions in $R_4Al_2O_9$-$R_4Si_2N_2O_7$-$R_4Si_2O_{10}$ (R=Y, Gd, Yb) systems

Yong Jiang, Zhenbang Wei, Wenzhou Sun, Limeng Liu, Zhenkun Huang

Pages 7588-7592

Purchase PDF Article preview

Research article *Open access*

Electrochemical performance of polymer-derived SiOC and SiTiOC ceramic electrodes for artificial cardiac pacemaker applications

Jongmoon Jang, Pradeep Vallachira Warriam Sasikumar, Fatemeh Navaee, Lorenz Hagelüken, ... Juergen Brugger

Pages 7593-7601

Download PDF Article preview

Research article ○ Abstract only

Optical properties of bismuth tellurite glasses doped with holmium oxide

C. Devaraja, G.V. Jagadeesha Gowda, B. Eraiah, K. Keshavamurthy

Pages 7602-7607

Purchase PDF Article preview

Research article ○ Abstract only

Spray pressure variation effect on the properties of CdS thin films for photodetector applications

A. Kathalingam, S. Valanarasu, Tansir Ahamad, Saad M. Alshehri, Hyun-Seok Kim

Pages 7608-7616

Purchase PDF Article preview

Research article ○ Abstract only

Effect of pre-oxidation and Al amount on the oxidation behavior of healing agents in YSZ-$Mo(Si_{1-x},Al_x)_2$ composite

Amin Majidi, Elena Navarrete-Astorga, José Ramón Ramos-Barrado, M.R. Rahimipour, M. Alizadeh

Pages 7617-7624

Purchase PDF Article preview

Research article ○ Abstract only

Direct ink writing of bismuth molybdate microwave dielectric ceramics

Athanasios Goulas, George Chi-Tangyie, Shiyu Zhang, Dawei Wang, ... Daniel S. Engstrøm

Pages 7625-7631

Ceramics International

Supports *open access*

6.1 CiteScore 3. In

Feihong Wang, Kunming Pan, Shizhong Wei, Yongpeng Ren, ... Qiaobao Zhang

Pages 7632-7641

Purchase PDF Article preview

Research article ○ Abstract only

Synthesis and Characterization of Hetero-metallic Oxides-Reduced Graphene Oxide Nanocomposites for Photocatalytic Applications

Rukia Fatima, Muhammad Farooq Warsi, Muhammad Ilyas Sarwar, Imran Shakir, ... Sonia Zulfiqar

Pages 7642-7652

Purchase PDF Article preview

Research article ○ Abstract only

Nanocomposite powders of hydroxyapatite-graphene oxide for biological applications

Camila C. Lopes, Wagner A. Pinheiro, Daniel Navarro da Rocha, José G. Neves, ... Marcelo H. Prado da Silva

Pages 7653-7665

Purchase PDF Article preview

Research article ○ Abstract only

Influence of Ag incorporation on the structural, optical and electrical properties of ITO/Ag/ITO multilayers for inorganic all-solid-state electrochromic devices

Hongli Wang, Chunmei Tang, Qian Shi, Mengyao Wei, ... Mingjiang Dai

Pages 7666-7673

Purchase PDF Article preview

Research article ○ Abstract only

High-density sol-gel derived, cold-isostatically pressed $La_{0.67}Ca_{0.27}Sr_{0.06}MnO_3$ polycrystalline ceramics and their room-temperature *TCR* improvement

Yang Liu, Gang Dong, Shuai Zhang, Xiang Liu

Pages 7674-7682

Purchase PDF Article preview

Research article ○ Abstract only

Study on the subsurface damage mechanism of optical quartz glass during single grain scratching

Ming Li, Xiaoguang Guo, Ruifeng Zhai, Xichun Luo, ... Dongming Guo

Pages 7683-7691

Purchase PDF Article preview

Research article ○ Abstract only

Integrated piezo-photocatalysis of electrospun $Bi_4Ti_3O_{12}$ nanostructures by bi-harvesting visible light and ultrasonic energies

Daiming Liu, Chengchao Jin, Yongtao Zhang, Yan He, Fei Wang

Pages 7692-7699

Purchase PDF Article preview

Ceramics International

Supports *open access*

6.1 CiteScore 3. In

Purchase PDF Article preview

Research article ○ Abstract only

Kinetics and in situ observation of nonisothermal crystallization in Bayan Obo tailing-based nanocrystalline glass-ceramic

Qingwei Bai, Yusheng Yang, Zengwu Zhao

Pages 7711-7719

Purchase PDF Article preview

Research article ○ Abstract only

Enhanced voltage endurance capability of $Ba(Zr_{0.2}Ti_{0.8})O_3$ thin films induced by atomic-layer-deposited Al_2O_3 intercalations and the application in electrostatic energy storage

Niefang Mao, Linghao Meng, Yawei Li, Zhigao Hu, Junhao Chu

Pages 7720-7727

Purchase PDF Article preview

Research article ○ Abstract only

Improvement of gas sensing property for two-dimensional $Ti_3C_2T_x$ treated with oxygen plasma by microwave energy excitation

Ming Hou, Shenghui Guo, Li Yang, Jiyun Gao, ... Yongxiang Li

Pages 7728-7737

Purchase PDF Article preview

Research article ○ Abstract only

Vitrification of municipal solid waste incineration fly ash: An approach to find the successful batch compositions

Elham Sharifikolouei, Francesco Baino, Milena Salvo, Tonia Tommasi, ... Monica Ferraris

Pages 7738-7744

Purchase PDF Article preview

Research article ○ Abstract only

Complex optimization of arc melting synthesis for bulk Cr_2AlC MAX-phase

Kirill Sobolev, Anna Pazniak, Oleg Shylenko, Vladimir Komanicky, ... Valeria Rodionova

Pages 7745-7752

Purchase PDF Article preview

Research article ○ Abstract only

Effect of SiC crystal orientation on Ti_3SiC_2formation between SiC and Al/Ti bi-layered film

Yasuo Takahashi, Masato Tsutaoka, Masakatsu Maeda

Pages 7753-7763

Purchase PDF Article preview

Research article ○ Abstract only

Facile synthesis of TiO_2-supported Al_2O_3 ceramic hollow fiber substrates with extremely high photocatalytic activity and reusability

Ceramics International

Supports *open access*

6.1 CiteScore 3. In

Scalable production of boron nitride nanosheets in ionic liquids by shear-assisted thermal treatment
Guoxun Sun, Jianqiang Bi
Pages 7776-7782

Purchase PDF Article preview

Research article ○ Abstract only

Preparation, structure and microwave dielectric properties of novel La_2MgGeO_6 ceramics with hexagonal structure and adjustment of its τ_f value
Xianjie Zhou, Kangguo Wang, Sang Hu, Xiaowen Luan, ... Huanfu Zhou
Pages 7783-7789

Purchase PDF Article preview

Research article ○ Abstract only

Effects of water atmosphere on chemical degradation of $PrBa_{0.5}Sr_{0.5}Co_{1.5}Fe_{0.5}O_{5+\delta}$ electrodes
Mingi Choi, Seo Ju Kim, Wonyoung Lee
Pages 7790-7797

Purchase PDF Article preview

Research article ○ Abstract only

Synthesis and physicochemical characterization of Zn-doped brushite
Aleksandra Laskus-Zakrzewska, Anna Zgadzaj, Joanna Kolmas
Pages 7798-7804

Purchase PDF Article preview

Research article ○ Abstract only

Biphasic bone graft prepared using a gel-foaming technique
Hao-Yu Chang, Ying-Cen Chen, Wei-Hsing Tuan, Sseu-Pei Hwang, ... Po-Liang Lai
Pages 7805-7813

Purchase PDF Article preview

Research article ○ Abstract only

Systematic study of an Fe_2O_3 stacked homojunction photoelectrochemical photoelectrode
Yaejin Hong, Seung-Hwan Jeon, Hyunjin Jeong, Hyukhyun Ryu
Pages 7814-7823

Purchase PDF Article preview

Research article ○ Abstract only

Microstructural evolution of carbon fibers by silicon vapor deposition and its effect on mullite-corundum castables
Si Ouyang, Yuanbing Li, Degang Ouyang, Shujing Li, ... Ruofei Xiang
Pages 7824-7830

Purchase PDF Article preview

Ceramics International

Supports *open access*

6.1 CiteScore 3. In

Research article ○ Abstract only

Synthesis of high-performance electrochromic thin films by a low-cost method

Yangbiao Liu, Jixi Wang, Xiudi Xiao, Xuesong Cai, ... Gang Xu

Pages 7837-7844

Purchase PDF Article preview

Research article ○ Abstract only

Flexible TiO_2 nanograss array film decorated with BiOI nanoflakes and its greatly boosted photocatalytic activity

Liang Hao, Yifei Hu, Yan Zhang, Xuecheng Ping, ... Jizi Liu

Pages 7845-7852

Purchase PDF Article preview

Research article ○ Abstract only

Effects of HfC/PyC core-shell structure nanowires on the microstructure and mechanical properties of $Hf_{1-x}Zr_xC$ coating

Jincui Ren, Yuting Duan, Chaofeng Lv, Jiyuan Luo, ... Yanqin Fu

Pages 7853-7863

Purchase PDF Article preview

Research article ○ Abstract only

Mechanical properties, electrical resistivity and piezoresistivity of carbon fibre-based self-sensing cementitious composites

Lining Wang, Farhad Aslani

Pages 7864-7879

Purchase PDF Article preview

Research article ○ Abstract only

Structure and properties of lightweight magnesia refractory castables with porous matrix

Chuang Jie, Hao Liu, Zhoufu Wang, Xitang Wang, Yan Ma

Pages 7880-7887

Purchase PDF Article preview

Research article ○ Abstract only

Influence of Cr and Fe doping on the structure, magnetic and optical properties of nano $CuCo_2O_4$

Zein K. Heiba, Noura M. Farag, A.M. El-naggar, Jasper R. Plaisier, ... Mohamed Bakr Mohamed

Pages 7888-7897

Purchase PDF Article preview

Research article ○ Abstract only

Effect of microstructure change on resistance of spherical $LiCoO_2$ to electrode degradation for proton intercalation

Jun Ping, Sajid Rauf, Zuhra Tayyab, Ruilong Wang, ... Changping Yang

Pages 7898-7905

Purchase PDF Article preview

Ceramics International

Supports *open access*

6.1 CiteScore 3. In

Research article ○ Abstract only

$Gd_3Al_3Ga_2O_{12}$:Ce, Mg^{2+} transparent ceramic phosphors for high-power white LEDs/LDs

Hui Ding, Zehua Liu, Yongfu Liu, Pan Hu, ... Jun Jiang

Pages 7918-7924

Purchase PDF Article preview

Research article ○ Abstract only

A multiscale modeling for predicting the thermal expansion behaviors of 3D C/SiC composites considering porosity and fiber volume fraction

Zheng Sun, Zhongde Shan, Tianmin Shao, Jiahua Li, Xiaochuan Wu

Pages 7925-7936

Purchase PDF Article preview

Research article ○ Abstract only

Optimization of microwave absorption properties of C/NiP microfiber composites

Yupeng Wei, Jingpeng Lin, Tiantian Jiang, Linqi Li, ... Yong Peng

Pages 7937-7945

Purchase PDF Article preview

Research article ○ Abstract only

Artificial intelligence density model for oxide glasses

Shaik Kareem Ahmmad, Nameera Jabeen, Syed Taqi Uddin Ahmed, Shaik Amer Ahmed, Syed Rahman

Pages 7946-7956

Purchase PDF Article preview

Research article ○ Abstract only

Characterization of free carbon forms in β-SiC nanopowders by temperature-programmed oxidation and Raman spectroscopy

Pavel V. Krasovskii, Sergey K. Sigalaev, Yuriy V. Grigoriev

Pages 7957-7965

Purchase PDF Article preview

Research article ○ Abstract only

Densification of silicon nitride powder by spark plasma extrusion

S.B. Alemán-Córdova, L. Ceja-Cárdenas, J.C. Méndez-García, S. Díaz-de la Torre

Pages 7966-7973

Purchase PDF Article preview

Research article ○ Abstract only

The enhanced visible light driven photocatalytic inactivation of Escherichia coli with Z-Scheme Bi_2O_3/Bi_2MoO_6 heterojunction and mechanism insight

Huanxian Shi, Cunjin Wang, Wei Wang, Xiaoyun Hu, ... Zhishu Tang

Ceramics International

Supports *open access*

6.1 CiteScore 3.

You-Dong Kim, Ja-Yoon Yang, Muhammad Saqib, Kwangho Park, ... Jun-Young Park

Pages 7985-7993

Purchase PDF Article preview

Research article ○ Abstract only

Improving optical and electrical performances of aluminum-doped zinc oxide thin films with laser-etched grating structures

Li-jing Huang, Lei Zhao, Bao-jia Li, Yao Zhang, ... Juan Song

Pages 7994-8003

Purchase PDF Article preview

Research article ○ Abstract only

Multifunction properties of SiOC reinforced with carbon fiber and in-situ SiC nanowires

Junjie Qian, Anze Shui, Chao He, Xuan Wang, ... Bin Du

Pages 8004-8013

Purchase PDF Article preview

Research article ○ Abstract only

Structural transformation in Mn-substituted $Sr_2Bi_2Ta_2TiO_{12}$ Aurivillius phase synthesized by hydrothermal method: A comparative study and dielectric properties

Ilona Bella, Tio Putra Wendari, Novesar Jamarun, Nandang Mufti, Zulhadjri

Pages 8014-8019

Purchase PDF Article preview

Research article ○ Abstract only

Microstructural evolution and phase transition mechanism of Ti(C,N)-based cermets during vacuum sintering process

Dingqian Dong, Wei Yang, Xin Xiang, Bo Huang, ... Kaihua Shi

Pages 8020-8029

Purchase PDF Article preview

Research article ○ Abstract only

Europium-activated phosphor $Ba_3Lu_2B_6O_{15}$: Influence of isomorphic substitution on photoluminescence properties

I.E. Kolesnikov, R.S. Bubnova, A.V. Povolotskiy, Y.P. Biryukov, ... S.K. Filatov

Pages 8030-8034

Purchase PDF Article preview

Research article ○ Abstract only

Synthesis and thermal evolution of polysilazane-derived SiCN(O) aerogels with variable C content stable at 1600 °C

Andrea Zambotti, Mattia Biesuz, Renzo Campostrini, Sara Maria Carturan, ... Gian Domenico Sorarù

Pages 8035-8043

Purchase PDF Article preview

Research article ○ Abstract only

Ceramics International

Supports *open access*

6.1 CiteScore 3. In

Research article ○ Abstract only

NiO–ZnO based junction interface as high-temperature contact materials

Temesgen D. Desissa

Pages 8053-8059

Purchase PDF Article preview

Research article ○ Abstract only

Effects of substrate temperature on thermal stability of Al-doped ZnO thin films capped by AlO_x

Hoa T. Dao, Hisao Makino

Pages 8060-8066

Purchase PDF Article preview

Research article ○ Abstract only

Optimisation on the stability of CaO-doped partially stabilised zirconia by microwave heating

Yeqing Ling, Qiannan Li, Hewen Zheng, Mamdouh Omran, ... Guo Chen

Pages 8067-8074

Purchase PDF Article preview

Research article ○ Abstract only

FEA evaluation of material stiffness changes for a polymer assisted 3D polycaprolactone/β-tricalcium phosphate scaffold in a mandibular defect reconstruction model

Baboucarr Lowe, Eero Huotilainen, Markku Laitinen, Anna-Maria Henell, ... Laurence J. Walsh

Pages 8075-8081

Purchase PDF Article preview

Research article ○ Abstract only

Fabrication of binary metal substituted CdO with superior aptitude for dye degradation and antibacterial activity

Abdur Rahman, Muhammad Aadil, Sonia Zulfiqar, Ibrahim A. Alsafari, ... Mahmoud E.F. Abdel-Haliem

Pages 8082-8093

Purchase PDF Article preview

Research article ○ Abstract only

Reaction induced multifunctional TiO_2 rod/particle nanostructured materials for screen printed dye sensitized solar cells

R. Selvapriya, V. Sasirekha, P. Vajeeston, J.M. Pearce, J. Mayandi

Pages 8094-8104

Purchase PDF Article preview

Research article ○ Abstract only

Microstructures and oxidation behaviors of Al-modified and Al_2O_3-modified SiC coatings on carbon/carbon composites via pack cementation

Jinguo Huang, Lingjun Guo, Kaijiao Li, Ningning Yan, ... Yunyu Li

Pages 8105-8112

Ceramics International

Supports *open access*

6.1 CiteScore 3.

Ceramics International

Supports *open access*

6.1 CiteScore

3. In

conditions; influence on the microstructure and composition at the different polarized interfaces

Hassan Javed, Kai Herbrig, Antonio Gianfranco Sabato, Domenico Ferrero, ... Federico Smeacetto

Pages 8184-8190

Download PDF Article preview

Research article ○ Abstract only

A high-temperature structural and wave-absorbing SiC fiber reinforced Si_3N_4 matrix composites

Ran Mo, Fang Ye, Xiaofei Liu, Qian Zhou, ... Laifei Cheng

Pages 8191-8199

Purchase PDF Article preview

Research article ○ Abstract only

Suitability of Biosilicate® glass-ceramic powder for additive manufacturing of highly porous scaffolds

Hamada Elsayed, Paolo Colombo, Murilo C. Crovace, Edgar D. Zanotto, Enrico Bernardo

Pages 8200-8207

Purchase PDF Article preview

Research article ○ Abstract only

Hydrothermally grown ZnO NSs on Bi-Directional woven carbon fiber and effect of synthesis parameters on morphology

Ravi Shankar Rai, Vivek Bajpai

Pages 8208-8217

Purchase PDF Article preview

Research article ○ Abstract only

A biotemplate synthesized hierarchical Sn-doped TiO_2 with superior photocatalytic capacity under simulated solar light

Jiao Li, Jiao Shi, Yuanbiao Li, Zhanlai Ding, Jianguo Huang

Pages 8218-8227

Purchase PDF Article preview

Research article ○ Abstract only

Effect of M^{3+} (M = Bi, Al) co-doping on the luminescence enhancement of $Ca_2ZnSi_2O_7:Sm^{3+}$ orange-red–emitting phosphors

Xi Shui, Chenyu Zou, Wentao Zhang, Chengshuai Bao, Yi Huang

Pages 8228-8235

Purchase PDF Article preview

ISSN: 0272-8842

Ceramics International

Supports *open access*

ELSEVIER

6.1 CiteScore

3. Im

Ceramics International 47 (2021) 8014–8019

Contents lists available at ScienceDirect

Ceramics International

journal homepage: www.elsevier.com/locate/ceramint

Structural transformation in Mn-substituted $Sr_2Bi_2Ta_2TiO_{12}$ Aurivillius phase synthesized by hydrothermal method: A comparative study and dielectric properties

Ilona Bella [a], Tio Putra Wendari [a], Novesar Jamarun [a], Nandang Mufti [b], Zulhadjri [a,*]

[a] Department of Chemistry, Universitas Andalas, Kampus Limau Manis, Padang, 25163, Indonesia
[b] Department of Physics, Universitas Negeri Malang, Jl. Semarang 5, Malang, 65145, Indonesia

ARTICLE INFO

Keywords:
Aurivillius phase
Hydrothermal method
Structural refinement
Dielectric properties
Ferroelectric transition

ABSTRACT

In this study, a hydrothermal method was applied to synthesize the three-layer Aurivillius phase $Sr_2Bi_2Ta_2TiO_{12}$ (SBTTO) and Mn-substituted $Sr_{1.5}Bi_{2.5}Ta_2Ti_{0.5}Mn_{0.5}O_{12}$ (SBTTMO), with the use of NaOH as a mineralizer. The crystal structure, morphology, dielectric properties, and the correlation between the structural transformation and dielectric properties were investigated. The XRD data reveal that the SBTTO sample adopts a tetragonal crystal structure with the *I4/mmm* space group and is then transformed into an orthorhombic structure with the *B2cb* space group for SBTTMO. The morphology of both samples was observed by SEM, which showed anisotropic plate-like grains. With the Mn substitution, the ferroelectric transition temperature (T_c) significantly increases as the influence of the $6s^2$ lone pair of Bi^{3+} increases, and this in turn further induces the relaxor-ferroelectric behavior. Consequently, the increase in T_c confirms the structural transformation from the paraelectric-tetragonal to the ferroelectric-orthorhombic phase.

1. Introductions

Ferroelectric material has the ability to change the value of electric polarization but remain in a switched state, even when the field is removed. These ferroelectric oxide materials are widely applied in electronic devices such as data storage (Fe-RAMs), energy storage, sensors, actuators, transducers and capacitors [1–4]. Among them, Aurivillius phases often exhibit excellent ferroelectric properties in nature, attributable to their structural properties. The Aurivillius phase represents the bismuth layered oxides with the general formula $[Bi_2O_2]^{2+}[A_{m-1}B_mO_{3m+1}]^{2-}$. The structure is constructed from perovskite-like layers $[A_{m-1}B_mO_{3m+1}]^{2-}$ and bismuth oxide layers $[Bi_2O_2]^{2+}$, stacked along the crystallographic *c*-axis, where *m* denotes the number of perovskite layers. The *A*-site cation in the perovskite-layers is occupied by mono-, di-, or trivalent cations (Na^+, K^+, Ca^{2+}, Sr^{2+}, Ba^{2+}, etc.) and the *B*-site cation is the transition metal with a high valency (Ti^{4+}, Nb^{5+}, Ta^{5+}, etc.) [5]. The crystal structure of the three-layer Aurivillius phase is depicted in Fig. 1a [6,7]. The perovskite-layer structure can accommodate a wide range of *A*- and *B*-site cation substitutions, allowing for control of the structure as well as of its physical properties. The Bi_2O_2 insulator layers and the distorted BO_6 octahedra in the perovskite layers play an essential role in terms of the ferroelectricity in the Aurivillius phases [8].

The majority of studies concentrated on the three-layer Aurivillius phases are focused on $Bi_4Ti_3O_{12}$, which adopts a non-centrosymmetric crystal structure with the *B2cb* space group, and exhibits a high dielectric constant with a high ferroelectric transition temperature (T_c) of 670 °C [9]. This pronounced ferroelectricity in $Bi_4Ti_3O_{12}$ is attributable to the effect of $6s^2$ lone pair electrons of Bi-rich content in the perovskite layers, which induce a highly distorted octahedral structure, as seen in Fig. 1b [10]. However, another member of the three-layer Aurivillius family with the general formula of $A_2Bi_2B_2TiO_{12}$ (A = Ca^{2+}, Ba^{2+}, Sr^{2+}; B = Nb^{5+}, Ta^{5+}) is reported to be paraelectric in nature since it possesses the *I4/mmm* tetragonal crystal structure (see Fig. 1) [11]. To date, research focused on the $Sr_2Bi_2Ta_2TiO_{12}$ compound is lacking.

In order to improve the ferroelectricity of the Aurivillius phase, the substitution of the smaller *A*-site cations with a d^0 shell is a feasible way to induce the distortion of BO_6 octahedra [12]. On the other hand, the substitution of *B*-site cations with the first-row transition cations with a half-filled *d*-shell (d^n) is well-known to promote magnetization and in turn exhibits the needed multiferroic properties [13,14]. Besides, the

* Corresponding author. Department of Chemistry, Universitas Andalas, Kampus Limau Manis, Padang, 25163, Indonesia
E-mail address: zulhadjri@sci.unand.ac.id (Zulhadjri).

https://doi.org/10.1016/j.ceramint.2020.11.154
Received 15 September 2020; Received in revised form 2 November 2020; Accepted 18 November 2020
Available online 21 November 2020

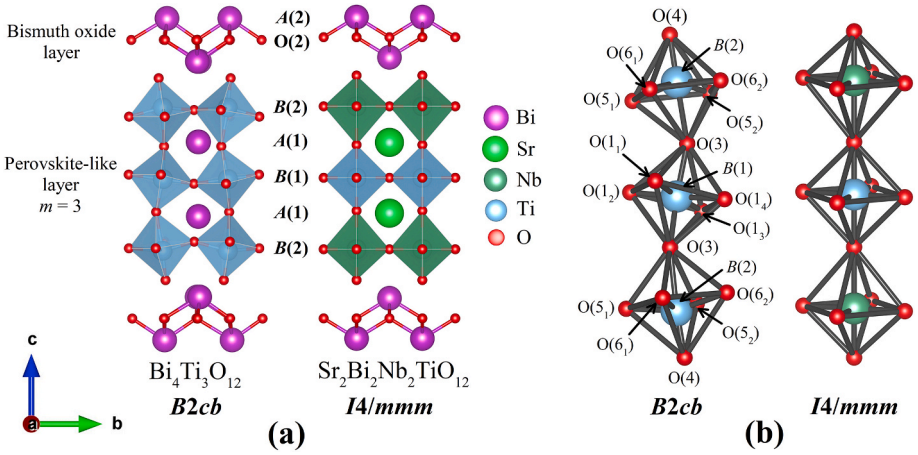

Fig. 1. (a) Crystal structure models of three-layer Aurivillius phases with *B*2*cb* and *I*4/*mmm* space group viewed along the *ac*-plane. (b) View of linked BO_6 octahedra projected along the *c*-axis. Atomic coordinates were taken from Refs. 6 and 7.

substitution of *B*-site cations with various ionic radii potentially enhances the structural distortion in BO_6 octahedra, thus improving its ferroelectricity [15,16]. The substitution of the Mn^{3+} cation (d^4) for the higher valence state cation (Nb^{5+} or Ti^{4+}) in the *B*-site cation was reported to improve the dielectric properties since it is compensated by the increase in Bi^{3+} contents to maintain the charge neutrality [8,17]. Therefore, the substitution of Mn^{3+} for Ti^{4+} in the $Sr_2Bi_2Ta_2TiO_{12}$ is expected to improve the ferroelectricity and raise the magnetization, which is especially useful for data storage applications.

The synthesis of the multiferroic Aurivillius phase is challenging since the different characters of d^0 and d^n ions with the various ionic radii possibly destroy the structure when partial substitutions are performed [18]. A conventional solid-state method is the most popular method applied in the preparation of the Aurivillius phase. However, the use of high-temperature sintering often results in the volatilization of Bi^{3+} and oxidation of the Mn^{3+} cation, leading to the formation of the impurity phase [13,19]. Therefore, the synthesis using a liquid-phase reaction medium such as the hydrothermal method likely favors the synthesis of the multiferroic Aurivillius phase at a low temperature. Hydrothermal synthesis involves the use of solvents with a temperature and pressure above the boiling point [4]. The oxide precursors increase the solubility of the solid and in turn accelerate the reaction rate. The use of hydrothermal synthesis can have many advantages such as high-pressure synthesis, lower-temperature synthesis, faster ionic diffusion, and well-controlled crystal growth and morphology [20]. Moreover, it is well-known that the compositional homogeneity and morphology significantly impact the physical properties [21,22].

In this work, the hydrothermal method was employed to report the synthesis of the Mn-substituted $Sr_2Bi_2Ta_2TiO_{12}$ phases with the chemical formula $Sr_{2-x}Bi_{2+x}Ta_2Ti_{1-x}Mn_xO_{12}$ ($x = 0$ and 0.5). The substitution of Mn^{3+} for Ti^{4+} was also compensated by the substitution of Bi^{3+} for Sr^{2+} to maintain overall charge neutrality. Therefore, we synthesized compounds of composition $Sr_2Bi_2Ta_2TiO_{12}$ and $Sr_{1.5}Bi_{2.5}Ta_2Ti_{0.5}Mn_{0.5}O_{12}$, abbreviated as SBTTO and SBTTMO, respectively. We investigate the relationships between the structure and its dielectric properties. The structure, morphology, and dielectric properties of both compounds were all considered.

1.1. Experimental procedures

The samples of $Sr_2Bi_2Ta_2TiO_{12}$ and $Sr_{1.5}Bi_{2.5}Ta_2Ti_{0.5}Mn_{0.5}O_{12}$ were prepared by the hydrothermal method, with $Sr(NO_3)_2$ (Merck, 99.9%), Bi_2O_3, TiO_2, Ta_2O_5, Mn_2O_3 (Aldrich, ≥ 99.9%) as precursors. Stoichiometric amounts of precursors were weighed and added to 60 mL of NaOH 3 M. The solution was stirred and then transferred into a 100 mL Teflon vessel before being placed into a stainless-steel autoclave. The

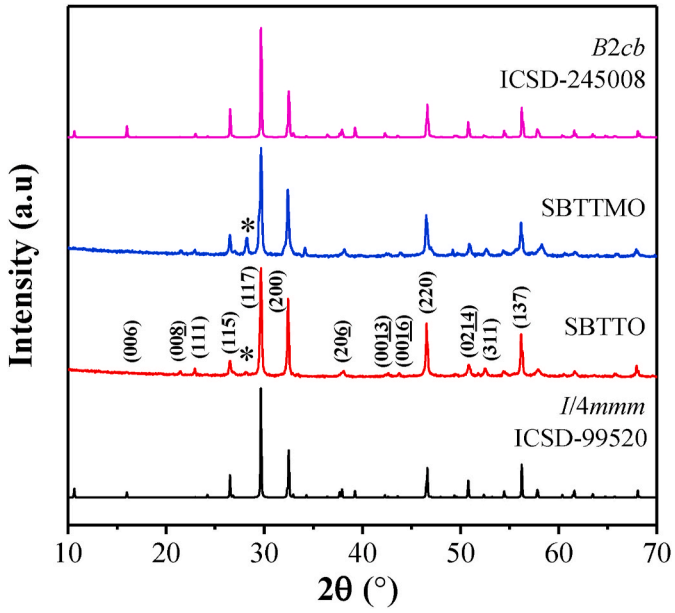

Fig. 2. X-ray diffraction patterns of SBTTO and SBTTMO samples indexed according to the standard three-layer Aurivillius phase with *I*4/*mmm* and *B*2*cb* space groups. Both samples exhibit a peak from an unidentified impurity phase.

samples were heated at a temperature of 240 °C for 120 h. The precipitates were filtered and then washed with deionized water to remove the base residue until pH 7 was recorded. The powder products were heated at 110 °C for 6 h, and calcined at 550 °C for 5 h and 900 °C for 4 h. XRD analysis was performed to investigate the formation of phase oxide and structural evolution using an X'Pert3 Powder PANalytical with Cu Kα radiation. The structures of the unit cells were determined by the Le Bail refinement technique, using the RIETICA program [23]. FTIR spectroscopy was carried out using a PerkinElmer 1600 FTIR spectrophotometer at room temperature. The surface morphology of the products was characterized by scanning electron microscopy (SEM; FEI INSPECT S50). The powders were then pressed into pellets and heated at 900 °C for 5 h to form a ceramic. The ceramic pellets were coated with silver paste (Aldrich, 99%) as electrodes. The temperature and frequency dependence of the dielectric properties were measured by using an LCR meter (BK Precision 891) with an amplitude of 1 V.

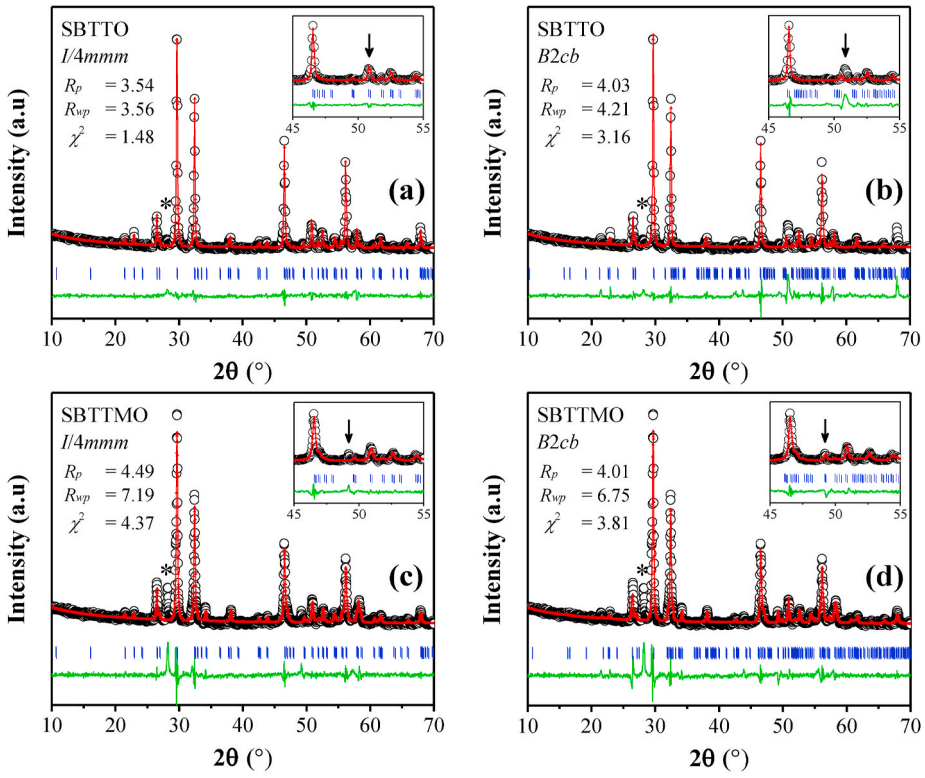

Fig. 3. Le Bail refinement fits of Aurivillius (a–b) SBTTO and (c–d) SBTTMO samples using the *I4/mmm* and *B2cb* space groups: experimental data (black circles), calculated data (red line), and difference data (green line). The blue tick marks indicate the positions of allowed Bragg reflections in each space group. (For interpretation of the references to colour in this figure legend, the reader is referred to the Web version of this article.)

2. Results and discussion

Fig. 2 depicts the X-ray diffraction patterns of Aurivillius SBTTO and SBTTMO samples synthesized using the hydrothermal method. The XRD patterns are compared to the standard diffraction data of the three-layer Aurivillius phase with the *I4/mmm* (ICSD-99520) and *B2cb* space groups (ICSD-245008). Since we investigate the effect of composition on the structure, we compare the samples using both space groups, which is commonly reported for the three-layer Aurivillius phase at room temperature [24]. This shows that XRD patterns match with the standard data, confirming the formation of the three-layer Aurivillius phase, while an unidentified impurity can be found at $2\theta = 28.17°$ for SBTTO and $2\theta = 29.23°$ for SBTTMO. The most intense diffraction peak (1 1 5) for all samples also reflects the formation of the three-layer Aurivillius phase ($m = 3$). This is in agreement with the fact that the most intense reflection is (1 1 $\underline{2m}\pm\underline{1}$) [25]. It was difficult to observe a difference in the peak to indicate the structural transformation.

To investigate the structure of the phase, the Le Bail refinement of the XRD data was performed with the RIETICA program to determine the structural phase and the lattice parameters [23]. The initial parameters for refinement were taken from the space group *I4/mmm* ($a = b = 3.8925$ Å, $c = 33.1876$ Å) (ICSD-99520) and *B2cb* ($a = 5.5051$ Å, $b = 5.5057$ Å, $c = 33.1947$ Å) (ICSD-245008). The parameters were automatically refined to obtain the optimal Le Bail profile and the value of the reliability factors (R_p, R_{wp}, χ^2), which are critical parameters for calculation accuracy, as shown in Fig. 3. In Fig. 3a, the XRD peaks of SBTTO were fitted with the *I4/mmm* space group. However, for the *B2cb* space group, the peak at $2\theta = 50.8°$ was not fitted, as shown in Fig. 3b. Moreover, the reliability factors also indicate the optimal value for the *I4/mmm* space group. These results suggest that the SBTTO sample has a tetragonal structure.

Subsequently, we also refined the overall structure of SBTTMO using both space groups, as depicted in Fig. 3c–d. The refinement results reveal that the good fits of SBTTMO were obtained for the *B2cb* space group. Meanwhile, for the *I4/mmm* space group, the peak at $2\theta = 49.1°$ could not be indexed by Bragg reflections. The reliability factors of the *B2cb* space group are also observed to be smaller than *I4/mmm*, which suggests the orthorhombic *B2cb* structure to be adopted in the SBTTMO sample at room temperature. The XRD data imply that the compositional-induced structural transformation is from tetragonal to orthorhombic in SBTTMO.

Table 1
Refined lattice parameters of the Aurivillius SBTTO and SBTTMO samples.

	SBTTO	SBTTMO
Space group	*I4/mmm*	*B2cb*
Crystal class	Tetragonal	Orthorhombic
a (Å)	3.8990(6)	5.5198(1)
b (Å)	3.8990(6)	5.5016(6)
c (Å)	33.1165(8)	33.1180(3)
V (Å^3)	503.461(8)	1005.735(7)
(*a*-*b*)/(*a*+*b*)	0	0.00165
Z	2	4
R_p	3.548	4.013
R_{wp}	3.560	6.715
χ^2	1.485	3.807

It was reported that the lone-pair effect of $6s^2$-electrons of Bi^{3+} ions in the perovskite layers is essential for the highly distorted BO_6 structure in the Aurivillius phases [8]. According to the nominal formula of $Sr_{2-x}Bi_{2+x}Ta_2Ti_{1-x}Mn_xO_{12}$, the substitution of Mn^{3+} for Ti^{4+} in SBTTMO increases the proportion of Bi^{3+} on the *A*-site, leading to a higher degree of structural distortion such as rotations and tilts of BO_6 octahedra, as demonstrated in Fig. 1b [26]. This distortion results in the break of inversion of the parent tetragonal structure, consequently giving rise to an orthorhombic structure [27].

Table 1 shows the refined lattice parameters obtained from the XRD

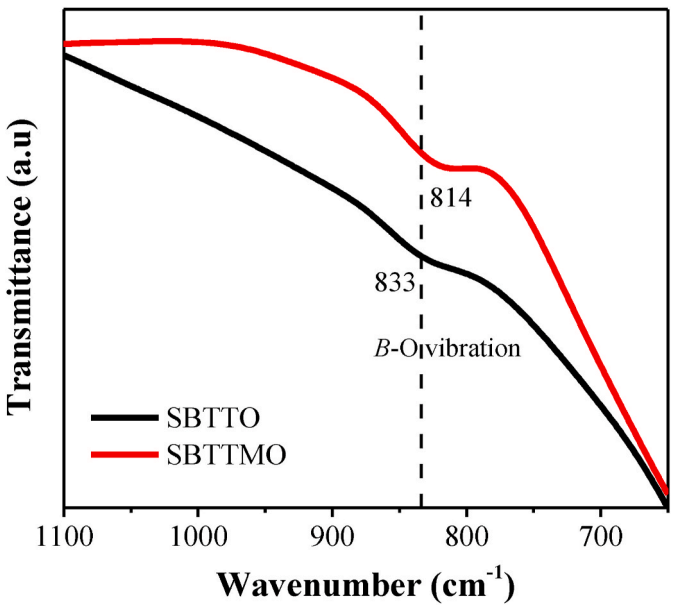

Fig. 4. FTIR spectra of Aurivillius SBTTO and SBTTMO samples at room temperature.

fit based on each space group. An increase in the degree of orthorhombic distortion in the SBTTMO sample leads to the difference between the *a* and *b* lattice parameters. This can also be expressed in terms of the orthorhombicity ratio $(a\text{-}b)/(a+b)$ in Table 1. In the Aurivillius phases with *B*2*cb* symmetry, the atomic displacement from the center of position in the *b*-axis gives rise to ferroelectricity [24]. This structural transformation can also be expected to increase the ferroelectric properties of the SBTTMO sample, as discussed hereafter.

Fig. 4 shows the IR spectra of the SBTTO and SBTTMO samples at room temperature from 650 to 1100 cm^{-1}. Both samples exhibit a phonon mode of ~833 cm^{-1}, ascribed to the *B*–O symmetric stretching mode of BO_6 octahedra [8]. The vibration mode of 833 cm^{-1} in SBTTO shifted toward the lower wavenumber of 814 cm^{-1} for SBTTMO. This is in agreement with Hooke's law since the bond strength of Mn–O (362 kJ/mol) is lower than that of Ti–O (666.5 kJ/mol) [8,28]. This result reveals that the Mn^{3+} cations incorporate into the BO_6 octahedra layers.

The grain morphologies of the SBTTO and SBTTMO samples observed using SEM are shown in Fig. 5a–b. The grain morphology is anisotropic and plate-like in nature and spreads evenly across all samples, which is a typical grain growth for the Aurivillius phases. It was found that the uniform grain size distribution can be obtained when using the hydrothermal method, unlike the high-temperature method [22,29]. The particle size distribution of SBTTO and SBTTMO was determined by ImageJ software, which is shown in Fig. 5c–d. The particle size of SBTTO is in the range of 0.21–1.28 μm, and is reduced in size with Mn^{3+} substitution to the range of 0.12–0.8 μm for SBTTMO. Moreover, the particle agglomeration is decreased and the particle shape becomes more uniform for the samples containing Mn^{3+} [18].

Fig. 6 depicts the temperature dependence of the dielectric constant (ϵ) and dielectric loss (tan δ) at a frequency range of 50 kHz–300 kHz. The dielectric properties of the samples were investigated for high frequencies, since this best reflects the intrinsic polarizability being correlated to the structural properties of the sample [17]. The magnitude of ϵ for SBTTO initially decreases with an increase in temperature, and then significantly increases above 350 °C, indicating that the sample becomes more conductive. This conductive behavior is also observed by the significant increase in the dielectric loss at this temperature. There is no ferroelectric-paraelectric transition peak (T_c) observed at this measured temperature, and the dielectric constant increases as the temperature decreases, suggesting that T_c is below room temperature. The T_c below RT was also previously observed in $Sr_2Bi_2TiNb_2O_{12}$, where the T_c of -136 °C is relevant [11]. This result confirms that the SBTTO exhibits paraelectric behavior in nature, which is in agreement with the centrosymmetric tetragonal structure of this sample.

For SBTTMO, the dielectric constant exhibits the single broad peak shown in Fig. 6b, corresponding to a phase transition from the ferroelectric to the paraelectric phase (T_c). The T_c peak of the SBTTMO sample indicates the predominance of the ferroelectric phase, according to a non-centrosymmetric orthorhombic structure with the *B*2*cb* space group. Furthermore, the T_c peak is between 300 °C and 350 °C, strongly depending on frequency (ΔT relaxation); this can be attributed to the contribution of the relaxor-ferroelectric behavior [30]. The dielectric

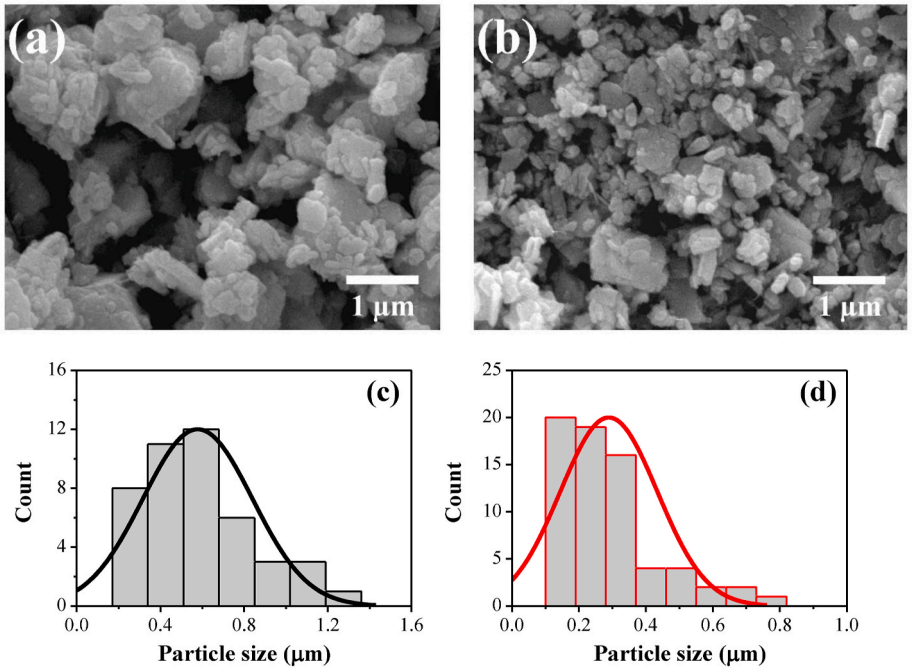

Fig. 5. SEM micrographs of Aurivillius (a) SBTTO and (b) SBTTMO samples. Particle size distribution of Aurivillius (c) SBTTO and (d) SBTTMO samples.

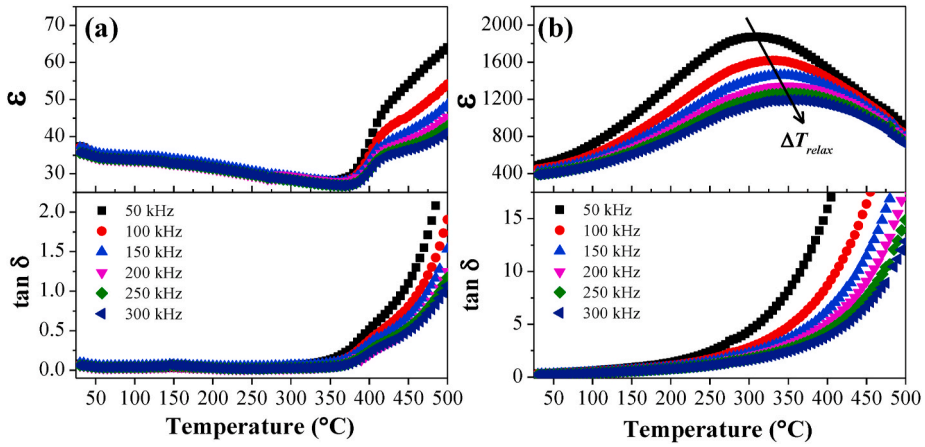

Fig. 6. Dielectric constant (ϵ) and dielectric loss (tan δ) of Aurivillius (a) SBTTO and (b) SBTTMO samples as a function of temperature at various frequencies.

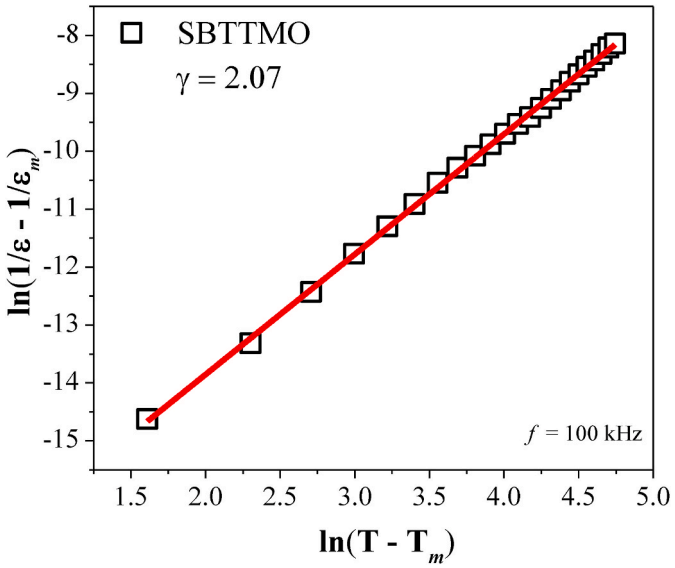

Fig. 7. A modified Curie-Weiss fitted line to quantify the degree of relaxor behavior for the SBTTMO sample.

loss increases with temperature, indicating the increased conductivity by thermal effects. Furthermore, the relaxor behavior in the SBTTMO sample was evaluated by the degree of diffuseness (γ) using a modified Curie-Weiss law [11]:

$$1/\varepsilon_r - 1/\varepsilon_m = (T - T_m)^\gamma / C$$

The γ value was obtained from the linear fitting to plots of $\ln(1/\epsilon_r - 1/\epsilon_m)$ versus $\ln(T\text{-}T_m)$, as shown in Fig. 7. This value is in the range of 1–2, where $\gamma = 1$ represents a normal ferroelectric behavior, while $\gamma = 2$ represents a relaxor-ferroelectrics behavior. The fitted value of γ is 2.07, which exhibits the pronounced relaxor behavior in SBTTMO with $\Delta(T_{m\,(300\ kHz)} - T_{m(50\ kHz)})$ of 50 °C. This is strongly induced by the increased compositional disorder of both *A*-site cation (Sr^{2+}/Bi^{3+}) and *B*-site cations ($Ta^{5+}/Ti^{4+}/Mn^{3+}$) [8,30]. This cation disorder causes the breaking of the long-range ferroelectric order into the polar nanoregion domain, and is thus reckoned to have a relaxor ferroelectric behavior.

Compared to the SBTTO, both the T_c and the magnitude of ϵ at 100 kHz significantly increase for SBTTMO, as shown in Table 2. The increased dielectric properties are attributed to an increase in the structural distortion, as discussed in the refinement results. This increase in the dielectric properties is also consistent with the lower Goldschmidt tolerance factor (t) of the perovskite layers of SBTTMO (0.950), compared to SBTTO (0.991), which is also related to the increase in T_c [31]. Therefore, the significant increase in T_c reveals the structural transformation from the paraelectric-tetragonal to the ferroelectric-orthorhombic phase (*I4/mmm* → *B2cb*), which is in agreement with the XRD study. It has been established that a non-centrosymmetric crystal structure gives rise to an electrical dipole moment, which may favor an increase of T_c. It is also found that the dielectric loss at room temperature significantly increases since the introduction of Mn^{3+} cation with unpaired electrons (d^4) in SBTTMO increases the charge transport [14].

3. Conclusion

The three-layer Aurivillius $Sr_2Bi_2Ta_2TiO_{12}$ (SBTTO) and $Sr_{1.5}Bi_{2.5}Ta_2Ti_{0.5}Mn_{0.5}O_{12}$ (SBTTMO) were synthesized by the hydrothermal method using NaOH 3 M as a mineralizer. The XRD data indicate the formation of the three-layer Aurivillius phase with an unidentified impurity phase in both samples. The Le Bail refinement from the XRD data confirms a structure transformation from tetragonal symmetry (*I4/mmm*) to an orthorhombic symmetry (*B2cb*), with the substitution of Mn^{3+} for Ti^{4+}. An anisotropic plate-like grain morphology with agglomeration was observed across all samples. The ferroelectric transition temperature (T_c) is below room temperature for SBTTO but significantly increases to 335 °C for SBTTMO at 100 kHz-; this is attributed to the increase in the structural distortion and a non-centrosymmetric crystal structure. Furthermore, the SBTTMO sample exhibits a pronounced relaxor-ferroelectric behavior driven by the increased disorder of the *A*-site cation (Sr^{2+}/Bi^{3+}) in the perovskite layer, as well as the *B*-site cations ($Ta^{5+}/Ti^{4+}/Mn^{3+}$).

Declaration of competing interest

The authors declare that they have no known competing financial

Table 2
Dielectric properties of the Aurivillius SBTTO and SBTTMO samples measured at 100 kHz.

Sample	ϵ_{RT}	tan δ (RT)	T_m (°C)	ϵ_m	tan δ (T_m)	Tolerance factor (t)	γ	ΔT_{relax} (°C)
SBTTO	37.03	0.072	< RT	–	–	0.991	–	–
SBTTMO	447.69	0.291	335	1618.22	4.027	0.950	2.07	50

interests or personal relationships that could have appeared to influence the work reported in this paper.

Acknowledgment

This work was supported by the Ministry of Research, Technology and Higher Education (RISTEKDIKTI) of The Republic of Indonesia through PMDSU Scholarship (050/SP2H/LT/DRPM/2018).

References

[1] P. Sun, H. Wang, X. Bu, Z. Chen, J. Du, L. Li, F. Wen, W. Bai, P. Zheng, W. Wu, L. Zheng, Y. Zhang, Enhanced energy storage performance in bismuth layer-structured $BaBi_2Me_2O_9$ (Me = Nb and Ta) relaxor ferroelectric ceramics, Ceram. Int. 46 (2020) 15907–15914, https://doi.org/10.1016/j.ceramint.2020.03.139.

[2] D. Zhao, I. Katsouras, M. Li, K. Asadi, J. Tsurumi, G. Glasser, J. Takeya, P.W. M. Blom, D.M. De Leeuw, Polarization fatigue of organic ferroelectric capacitors, Sci. Rep. 4 (2014) 1–7, https://doi.org/10.1038/srep05075.

[3] B.H. Park, B.S. Kang, S.D. Bu, T.W. Noh, J. Lee, W. Jo, Lanthanum-substituted bismuth titanate for use in non-volatile memories, Nature 401 (1999) 682–684.

[4] A. Moure, Review and perspectives of Aurivillius structures as a lead-free Piezoelectric system, Appl. Sci. 8 (2018), https://doi.org/10.3390/app8010062.

[5] B. Aurivillius, Mixed bismuth oxides with layer lattices 1. The structure type of $CaNb_2Bi_2O_9$, Ark. For Kemi. 1 (1949) 463–480.

[6] A. Shrinagar, A. Garg, R. Prasad, S. Auluck, Phase stability in ferroelectric bismuth titanate : a first-principles study, Acta Crystallogr. A 64 (2008) 368–375, https://doi.org/10.1107/S0108767308004601.

[7] M.S. Haluska, S.T. Misture, Crystal structure refinements of the three-layer Aurivillius ceramics $Bi_2Sr_{2-x}A_xNb_2TiO_{12}$ (A = Ca, Ba, x = 0, 0.5, 1) using combined X-ray and neutron powder diffraction, J. Solid State Chem. 177 (2004) 1965–1975, https://doi.org/10.1016/j.jssc.2004.01.010.

[8] T.P. Wendari, S. Arief, N. Mufti, V. Suendo, A. Prasetyo, Ismunandar, J. Baas, G. R. Blake, Zulhadjri, Synthesis, structural analysis and dielectric properties of the double-layer Aurivillius compound $Pb_{1-2x}Bi_{1.5+2x}La_{0.5}Nb_{2-x}Mn_xO_9$, Ceram. Int. 45 (2019) 17276–17282, https://doi.org/10.1016/j.ceramint.2019.05.285.

[9] A. Pelaiz-Barranco, Y. Gonzalez-Abreu, Ferroelectric ceramic materials of the Aurivillius family, J. Adv. Dielectr. 3 (2013) 1330003, https://doi.org/10.1142/S2010135X1330003X.

[10] A. Faraz, N. Deepak, M. Schmidt, M.E. Pemble, L. Keeney, A study of the temperature dependence of the local ferroelectric properties of c-axis oriented $Bi_6Ti_3Fe_2O_{18}$ Aurivillius phase thin films : illustrating the potential of a novel lead-free perovskite material for high density memory applications, AIP Adv. 5 (2015), 087123, https://doi.org/10.1063/1.4928495.

[11] T.W. Surta, A. Manjón-Sanz, E.K. Qian, R.H. Mansergh, T.T. Tran, L.B. Fullmer, M. R. Dolgos, Dielectric and ferroelectric properties in highly substituted $Bi_2Sr(A)TiNb_2O_{12}$ (A = Ca^{2+}, Sr^{2+}, Ba^{2+}) Aurivillius phases, Chem. Mater. 29 (2017) 7774–7784, https://doi.org/10.1021/acs.chemmater.7b02151.

[12] Q. Chang, H. Fan, C. Long, Effect of isovalent lanthanide cations compensation for volatilized A-site bismuth in Aurivillius ferroelectric bismuth titanate, J. Mater. Sci. Mater. Electron. 28 (2017) 4637–4646, https://doi.org/10.1007/s10854-016-6102-0.

[13] R. Ti, C. Wang, H. Wu, Y. Xu, C. Zhang, Study on the structural and magnetic properties of Fe/Co co-doped $Bi_4Ti_3O_{12}$ ceramics, Ceram. Int. 45 (2019) 7480–7487, https://doi.org/10.1016/j.ceramint.2019.01.040.

[14] T.P. Wendari, S. Arief, N. Mufti, A. Insani, J. Baas, G.R. Blake, Zulhadjri, Structural and multiferroic properties in double-layer Aurivillius phase $Pb_{0.4}Bi_{2.1}La_{0.5}Nb_{1.7}Mn_{0.3}O_9$ prepared by molten salt method, J. Alloys Compd. 820 (2020) 153145, https://doi.org/10.1016/j.jallcom.2019.153145.

[15] Q. Wang, C.M. Wang, Enhanced piezoelectric properties of Mn-modified $Bi_5Ti_3FeO_{15}$ for high-temperature applications, J. Am. Ceram. Soc. 103 (2020) 2686–2693, https://doi.org/10.1111/jace.16978.

[16] Y. Lu, H. Sun, Z. Wang, X. Xie, T. Yao, J. Wang, Y. Qi, X. Chen, Y. Lu, Improved room-temperature multiferroicity in Co-doped Aurivillius $Sr_{0.5}Bi_{5.5}Fe_{1.5}Ti_{3.5}O_{18}$ ceramics, J. Mater. Sci. Mater. Electron. 31 (2020) 1034–1046, https://doi.org/10.1007/s10854-019-02614-0.

[17] Zulhadjri, T.P. Wendari, U. Septiani, S. Arief, Investigation on structure, dielectric and magnetic properties of the four-layer Aurivillius phase $Pb_{1-x}Bi_{3.5+x}Nd_{0.5}Ti_{4-x}Mn_xO_{15}$ prepared via molten salt method, J. Solid State Chem. 292 (2020) 121723, https://doi.org/10.1016/j.jssc.2020.121723.

[18] Zulhadjri, A.A. Billah, T.P. Wendari, Emriadi, U. Septiani, S. Arief, Synthesis of Aurivillius Phase $CaBi_4Ti_4O_{15}$ doped with both La^{3+} and Mn^{3+} cations: crystal structure and dielectric properties, Mater. Res. 23 (2020), e20190521, https://doi.org/10.1590/1980-5373-MR-2019-0521.

[19] A. Khokhar, P.K. Goyal, O.P. Thakur, K. Sreenivas, Effect of excess of bismuth doping on dielectric and ferroelectric properties of $BaBi_4Ti_4O_{15}$ ceramics, Ceram. Int. 41 (2015) 4189–4198, https://doi.org/10.1016/j.ceramint.2014.12.103.

[20] Z. Xu, R. Chu, J. Hao, Z. Yao, H. Li, Hydrothermal preparation and electrical properties of Aurivillius phase $SrBi_4Ti_4O_{15}$ ceramic, Ferroelectrics 516 (2017) 148–155, https://doi.org/10.1080/00150193.2017.1362212.

[21] S. Niu, R. Zhang, X. Zhang, J. Xiang, C. Guo, Morphology-dependent photocatalytic performance of $Bi_4Ti_3O_{12}$, Ceram. Int. 46 (2020) 6782–6786, https://doi.org/10.1016/j.ceramint.2019.11.169.

[22] T.P. Wendari, S. Arief, N. Mufti, J. Baas, G.R. Blake, Zulhadjri, Ratio effect of salt fluxes on structure, dielectric and magnetic properties of La,Mn-doped $PbBi_2Nb_2O_9$ Aurivillius phase, Ceram. Int. 46 (2020) 14822–14827, https://doi.org/10.1016/j.ceramint.2020.03.007.

[23] B.A. Hunter, Rietica - a Visual Rietveld Program, Australian Nuclear Science and Technology Organisation, Australia, 2000.

[24] Q. Zhou, B.J. Kennedy, M.M. Elcombe, Synthesis and structural studies of cation-substituted Aurivillius phases $ASrBi_2Nb_2TiO_{12}$, J. Solid State Chem. 179 (2006) 3744–3750, https://doi.org/10.1016/j.jssc.2006.08.009.

[25] Z. Peng, X. Zeng, F. Cao, X. Yang, Microstructure and impedance properties of La, Ce multi-rare earth ions doped $Na_{0.5}Bi_{2.5}Nb_2O_9$ Aurivillius type ceramics, J. Alloys Compd. 695 (2017) 626–631, https://doi.org/10.1016/j.jallcom.2016.11.127.

[26] K.S. Aleksandrov, J. Bartolomé, Structural distortions in families of perovskite-like crystals, Phase Transitions 77 (2001) 255–335, https://doi.org/10.1080/01411590108228754.

[27] W.C. Ferreira, G.L.C. Rodrigues, B.S. Araújo, F.A.A. de Aguiar, A.N.A. de Abreu Silva, P.B.A. Fechine, C.W. de Araujo Paschoal, A.P. Ayala, Pressure-induced structural phase transitions in the multiferroic four-layer Aurivillius ceramic $Bi_5FeTi_3O_{15}$, Ceram. Int. 46 (2020) 18056–18062, https://doi.org/10.1016/j.ceramint.2020.04.122.

[28] Y. Luo, Comprehensive Handbook of Chemical Bond Energies, first ed., CRC Press, Boca Raton, 2007 https://doi.org/10.1201/9781420007282.

[29] P. Pookmanee, P. Uriwilast, S. Phanichpant, Hydrothermal synthesis of fine bismuth titanate powders, Ceram. Int. 30 (2004) 1913–1915, https://doi.org/10.1016/j.ceramint.2003.12.043.

[30] H. Du, Y. Li, H. Li, X. Shi, C. Liu, Relaxor behavior of bismuth layer-structured ferroelectric ceramic with m = 2, Solid State Commun. 148 (2008) 357–360, https://doi.org/10.1016/j.ssc.2008.05.017.

[31] D.Y. Suárez, I.M. Reaney, W.E. Lee, Relation between tolerance factor and T_c in Aurivillius compounds, J. Mater. Res. 16 (2001) 3139–3149, https://doi.org/10.1557/JMR.2001.0433.